Archives of Mechanics • Archiwum Mechaniki Stosowanej • 30, 4–5, pp. 531–551, Warszawa 1978

Symmetric and asymmetric vortices from inclined bodies of revolution — theory and experiment

J. N. NIELSEN and M. R. MENDENHALL (MOUNTAIN VIEW)

A SERIES of flow velocity measurements have been made at low speeds in several crossflow planes of an ogival cylinder at angles of attack of 22.4° and 37.5°. These flow velocities were obtained using a two-component laser anemometer in the 7- by 10-Foot Wind Tunnel of the Ames Research Center of NASA. The body vortices were approximately symmetrical at 22.4° angle of attack. Sufficient measurements were taken to determine the distribution of vorticity in the cross-flow plane. The general results of this investigation show that the vortices are not concentrated, and that the vorticity is well spread out. This is particularly true near the base of the model. Available theoretical methods for determining vortex strengths and positions and the resulting crossflow velocity field have serious shortcomings. Accordingly, a theory has been developed to overcome these shortcomings. The theory uses multiple vortex shedding and calculates the separation points on the body for both symmetric vortices. A number of comparisons is shown between the theory and the experiment with generally good agreement.

Wykonano szereg pomiarów prędkości przepływu przy niskich prędkościach w kilku płaszczyźnach przekroju pływu ostrołukowego cylindra przy kątach natarcia 22.4° i 37.5°. Prędkości przepływu otrzymano za pomocą dwuskładnikowego anemometru laserowego w tunelu aerodynamicznym o rozmiarach 7 na 10 stóp, znajdującym się w Ośrodku Badań Amesa firmy NASA. Wiry wokół ciała były w przybliżeniu symetryczne przy kącie natarcia 22.4°. Dokonano wystarczającej liczby pomiarów do określenia rozkładu wirowości w płaskim przepływie poprzecznym. Ogólne wyniki tego studium wykazują, że zawirowania nie są skoncentrowane i że wirowość może dobrze się rozprzestrzeniać. Jest to szczególnie widoczne w otoczeniu podstawy modelu. Dostępne metody teoretyczne, służące do określenia wytrzymałości i lokalizacji wirów oraz wypadkowych pól prędkości przekroju przepływu, mają poważne braki. Dlatego też opracowano teorię umożliwiającą ich usunięcie. W teorii tej wykorzystuje się wielokrotne powstawanie wirów i oblicza punkty odrywania się strug na ciele dla obydwu rodzai zawirowań symetrycznych i asymetrycznych. Przeprowadzono wiele porównań między teorią i eksperymentem. Otrzymano bardzo dobrą zgodność wyników teoretycznych i eksperymentalnych.

Проведен ряд измерений скорости течения, при низких скоростях, в нескольких плоскостях сечения течения стрельчатого цилиндра при углах атаки 22,4° и 37,5°. Скорости течения получены при помощи двухкомпонентного лазерного анемометра в аэродинамической трубе, с размерами 7 × 10 футов, находящейся в Центре Исследований Эймеса НАСА. Вихри вокруг тела были в приближении симметричными при угле атаки 22,4°. Проведено достаточное количество измерений для определения распределения вихрей в плоском поперечном течении. Общие результаты этого исследования показывают, что вихри не концентрированы и что завихренность может хорошо распространяться. Это особенно видно в окрестности основы модели. Доступные теоретические методы, служащие для определения стойкости и локализации вихрей, а также результирующих полей скорости сечения течения, имеют существенные недостатки. Поэтому разработана теория дающая возможность их устранения. В этой теории используется многократное рождение вихрей и вычисляются точки отрыва струй не теие для обоих родов симметричных и асимметричных вихрей. Проведено мног осравнений между теорией и экспериментом. Получено очень хорошее совпадение теоретических и экспериментальных результатов.

Nomenclature

C_p pressure coefficient, $\frac{p-p_{min}}{q_{min}}$,
D body diameter,
L body length,
M_∞ free-stream Mach number,
p local static pressure,
p_{min} static pressure at minimum pressure point,
q_{min} dynamic pressure at minimum pressure point,
R body radius,
ΔR distance from body surface to vortex starting position,
Re_ξ Reynolds number based on length ξ,
V, W velocity components along the axes of Y and Z, respectively,
v velocity in boundary layer tangent to body surface,
V_∞ free-stream velocity,
X, Y, Z body axes; X positive from body nose rearward along body axis of rotation, Y positive to right in horizontal direction; Z positive upward normal to X,
V_δ boundary-layer edge velocity in plane normal to axis of X,
ΔX integration interval along X-axis,
α body angle of attack,
β body of angle of sideslip,
δ boundary-layer thickness,
Γ strength of shed vorticity,
$\frac{d\Gamma}{dX}$ rate of vortex shedding per unit length along X,
ξ boundary-layer length in crossflow plane measured from virtual origin,
Λ empirical constant accounting for fraction of shed vorticity captured in recirculating region,
θ_s angular position of separation point, Fig. 11.

1. Introduction

A FLUID mechanical problem which has been of much interest over the years is the flow past a circular cylinder in a uniform stream. The well-known von Kármán vortex street is one important physical phenomenon occurring in such flows. It has been known for some time that the flow in planes normal to the axis of an inclined body of revolution has many of the physical features of a flow normal to circular cylinders. Figure 1 illustrates the vortex sheets associated with flow over a body of revolution at low and intermediate angles of attack. At low angles of attack the flow separates along two separation lines on the leeward side of the body. Vorticity sheets are formed by the boundary-layer fluid leaving the body surface at the separation lines and rolling up into a symmetrical vortex pair at their terminus. At higher angles of attack, an asymmetric vortex pattern is formed. At point P in Fig. 1 the vortex sheet breaks away from the body forming a free vortex. A new vortex sheet starts forming immediately. In this fashion, a series of free vortices of alternate sign are generated. It is intuitively clear that if the flow is viewed in a plane normal to the body axis far downstream, a vortex pattern similar to the von Kármán vortex street will appear. THOMSON and MORRISON [1] have used the von Kármán vortex

street analogy to correlate vortex shedding data on bodies of revolution at high angles of attack.

Because of the use of high angles of attack in aeronautical applications, the problem of the flow over bodies at such angles has assumed increased importance in recent years.

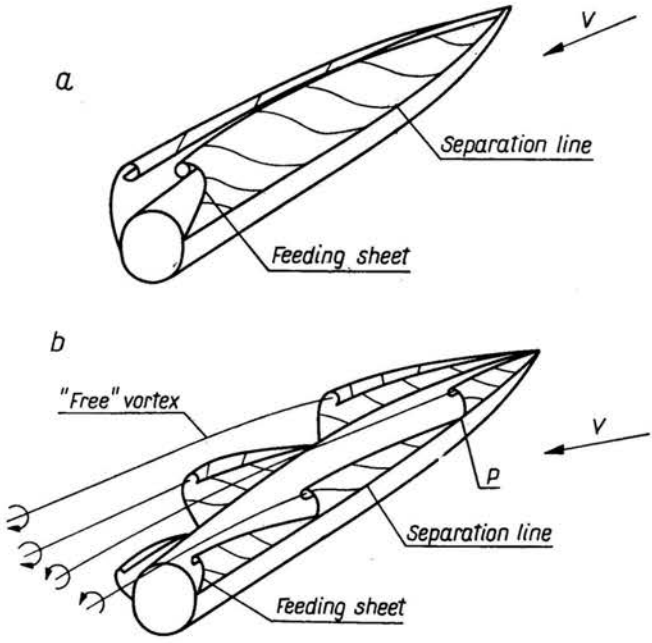

FIG. 1. Vortex formation on an inclined body of revolution.
a) Low angles of attack. b) Moderate angles of attack.

At the same time, means for investigating flow fields have improved. In particular, the use of the laser Doppler velocimeter (LDV) permits good flow measurements to be made in wind tunnels without disturbing the flow itself. Further, the capacity and speed of modern computers permits the use of sophisticated analytical models for predicting the flow field. This paper will address both of these subjects.

In the paper we will first describe the results of a body vortex investigation which was made using an LDV. Next we shall compare some of the measurements with simple available predictive methods to illustrate their limitations. Then, a more sophisticated model of the vortex flow field using "vortex clouds" will be described, and its predictions will be compared with experiment.

This study was sponsored in part by the U. S. A. Army Missile Command, with all experimental equipment being supplied by the NASA/Ames Research Center. Particular thanks are due to Dr. K. ORLOFF of the Large-Scale Aerodynamics Branch for the use of his laser anemometer, to the same branch for the use of the 7- by 10-Foot Wind Tunnel, and to the Aerodynamics Branch for the use of the model. The vortex-cloud theory was developed under the sponsorship of the Office of Naval Research.

2. Relevant work of other investigators

A large number of investigators have contributed to the knowledge of flow past circular cylinders and inclined bodies of revolution. A complete account of their work is not contemplated here. Rather a brief account is given of the results obtained by few of the workers whose contributions are particularly relevant to our purpose.

One of the interesting early models for a symmetric vortex pair in the presence of a two-dimensional circular cylinder is that due to FÖPPL [2]. Assuming potential flow past the cylinder and a symmetrical vortex pair, he was able to find a locus of vortex centers together with a specific vortex strength for each center such that the vortex pair was stationary in the presence of the cylinder. This model does not apply to a vortex pair whose strength is growing with time so that no account of the vortex feeding sheet is taken. However, the solution is a simple and interesting one for comparison with data.

Turning now to three-dimensional models, an interesting example is that of BRYSON [3] who takes account of the vortex feeding sheets. His model appears in the following sketch. In order to determine vortex strengths and paths, Bryson used the conditions that the separation point is a stagnation point of the flow and that there is no net force

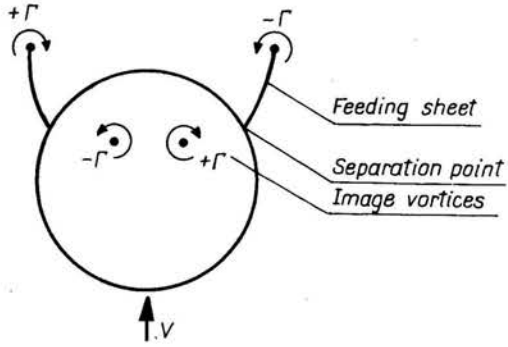

on the external vortex and its feeding sheet. The first condition yields an algebraic relationship, and the second one a differential equation between vortex strength and position. This condition as well as the vortex equations of motion yield the vortex path and strength. Good agreement between experiment and theory was obtained for an impulsively started cylinder in normal flow for the early stage of the impulsive motion. The special treatment of the vortex starting problem is noteworthy.

While models of the foregoing kind have been very useful in engineering prediction methods, they are only approximations to the actual wake flow. One way of making the models more realistic is to consider that the vorticity is not wholly concentrated in a single vortex pair, and to utilize more than one vortex per side to represent the cylinder vortical wake including the feeding sheets. One multivortex potential model of this kind is due to ANGELUCCI [4]. He considers a small feeding sheet for the vorticity close to the body and discrete vortices for earlier shed vorticity. He assumes, as Bryson, that the separation point is a stagnation point in the crossflow plane. As an additional condition, the feeding sheet is oriented in the direction of the local streamline. Angelucci advocates the use of

experimental data for the separation point locations as input to the calculative method. His method applies to non-circular bodies which can be transformed into the unit circle.

Another way in which the flow model can be improved is to use some viscous input, experimental or analytical, into the model to obtain better vortex strength and separation locations. WARDLAW [5] made this important step by using experimental vortex separation points. The vortex strengths were determined from boundary-layer considerations of the kind described in Sect. 5.3. The method is not well adapted to asymmetric vortices because the experimental separation point data are meager for this case, but it seems to give good predictions of the onset of vortex asymmetry as shown by KUHN [6].

The most significant step taken to extend the model to asymmetric vortices was to use boundary-layer techniques to determine the separation point locations as well as the vorticity shedding rates. This step was taken by MARSHALL and DEFFENBAUGH [7] using the boundary-layer separation criterion to determine the separation points. For both laminar and turbulent separation, STRATFORD gave separation criteria based on the pressure distribution which acts on the boundary layer [8 and 9]. The vortex-cloud theory discussed later in this report is based on the general approach of Marshall and Deffenbaugh with certain additions, subsequently described.

3. Experimental work

3.1. Test and equipment

The experiment has been described in Refs. [10 and 11], but a short account of it is repeated here for the sake of completeness. A similar experiment has recently been completed by YANTA and WARDLAW [12].

The test was performed in the NASA/Ames Research Center 7- by 10-Foot Wind Tunnel No. 1. It has a 46- by 59-inch window of optical quality plate glass opposite the model location. The LDV measurements were made through this window. The main components of the test apparatus are shown in Fig. 2. Located inside the tunnel were the body of revolution, its mounting, and a mirror which was mounted on the tunnel traversing mechanism (see the coordinate systems in Fig. 2). The LDV was located outside the tunnel, mounted on its own traversing mechanism.

The body of revolution used for the test was the 15.24 cm (6 in.) diameter missile body of the Ames Aerodynamics Branch. It has a 3.5 length-to-diameter ratio ogive nose with a sharp point (nose apex total angle of 32.9°) and the same length afterbody. Therefore, the total length of the body was 106.7 cm. The sting which held the body via the balance was a heavy-walled 5.7 cm (2-1/4 in.) diameter tube. It pivoted on a post, which was welded to the tunnel floor. The pitch angle was set by a linear actuator attached between the rear of the sting and the post, and this angle was sensed by a calibrated selsyn unit.

The LDV employed in this test was a two-component, backscatter type employing a 4-watt argon laser. This entire LDV could be traversed in the tunnel axial and vertical directions.

The two velocity components perpendicular to the axis of the four beams emitted from the LDV were sensed by Doppler frequency shifts of the scattered light since knowledge

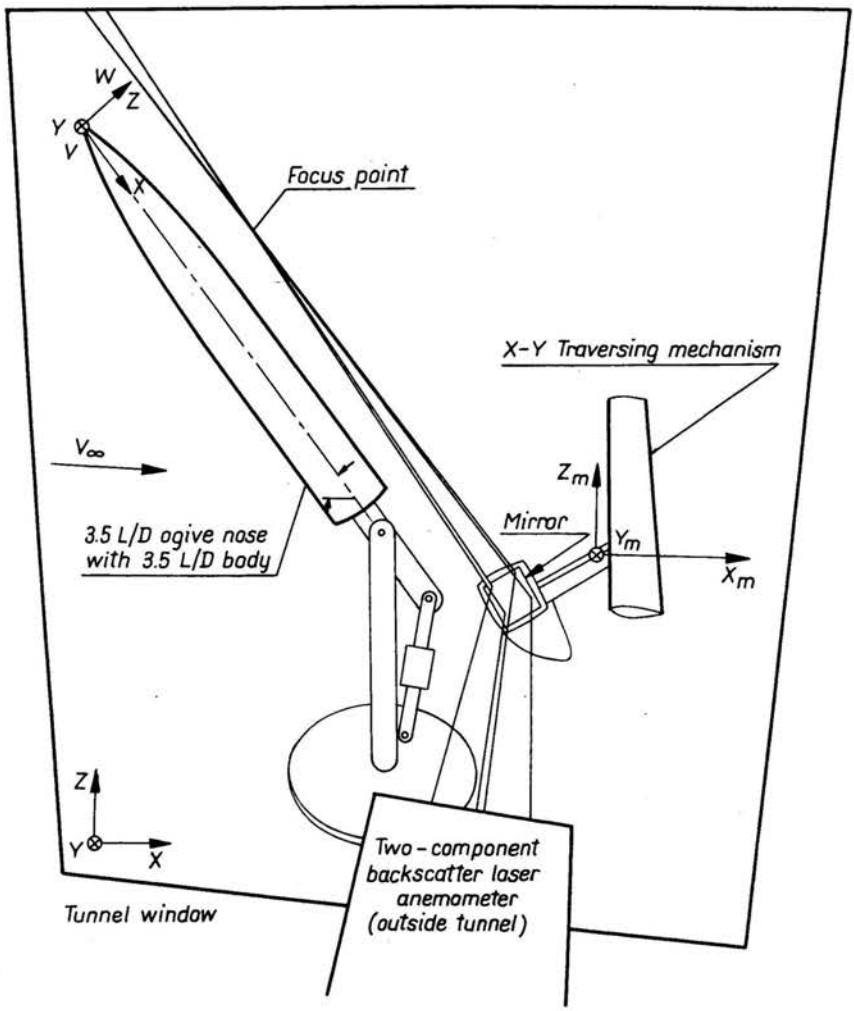

FIG. 2. Wind tunnel installation of LDV to obtain missile crossflow velocities.

of the flow pattern in the plane perpendicular to the body axis was required. It was necessary that the LDV beams be turned 90° by a mirror mounted in the tunnel behind the body (the reflected beams were also rotated about their axis). The mirror mount required two angular degrees of freedom for adjusting to different body pitch angles and two translational degrees of freedom for traversing the LDV focus point. Thus, a 10- by 12.6-cm (4- by 5-in.) front surfaced mirror was clamped to a plate and bracket to allow angular adjustments, and this was, in turn, mounted to the 7- by 10-Foot Wind Tunnel traversing mechanism. To make best use of the available range of local length of the LDV, the missile was placed off the wind tunnel centerline at 0.885 m (2.90 ft), or 5.8 body diameters, from the side wall of the tunnel closest to the LDV.

A 1.2-m (4 ft) long by 1-cm (0.4 in.) diameter tube containing a smoke generator with the smoke emitted from the tip was available. The smoke generator was mounted down-

stream of the body and operated continuously while operating the LDV to create fog in the tunnel. This provided the particles for scattering the light of the laser beams, creating a large flux of Doppler-shifted signals. However, it was found during testing that near the vortex centers few particles were available to give appropriate signals. The particles had apparently been centrifuged out by the rotary flow. This problem is well known in LDV work.

All data were obtained at a nominal free-stream velocity of 18.6 m/sec (61.0 ft/sec) which corresponds to a Reynolds number based on the missile diameter of 187,000. This velocity was selected as a compromise between decreasing LDV signal quality with an increasing Reynolds number.

The LDV data were obtained at pitch angles of 22.4° and 37.5°, at the 70 percent and 100 percent axial stations. The 22.4° pitch angle was selected to represent one near the maximum pitch angle for a symmetric vortex pair. The 37.5° pitch angle was selected after some difficulty to represent the minimum pitch with steady, asymmetric flow. However, even at that angle it was necessary to add a strip of tape 0.056 cm (0.022 in.) thick to the $-Y$ side of the nose with dimensions as indicated in the following sketch to assure a steady wake flow:

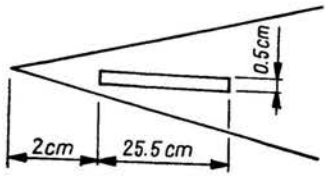

The details of the data are to be found in Ref. [13].

3.2. Presentation of overall flow field

As an example of the flow-field measurements, a velocity vector plot is presented in Fig. 3 for the plane normal to the body axis at 70 percent of the body length behind the nose for $\alpha = 22.4°$. A flow field stagnation point is visible on the vertical axis. Two well-defined vortices are indicated. The vortex core positions have been determined approximately from the condition that the core position is a stagnation point in the crossflow plane. The core positions so determined are not precisely symmetrical. While part of this asymmetry is no doubt due to experimental error, precise symmetry is not to be expected. It is noted that data near the vortex cores were difficult to obtain because smoke particles are centrifuged out of the core.

In Fig. 4 similar results are shown for the crossflow velocity field at the base of the body. Rather better coverage of the core region was obtained here possibly because of the more diffuse vorticity field at the base.

A widely used engineering method for calculating flows such as those shown in Figs. 3 and 4 is to replace the actual vortices by a pair of symmetric potential vortices using either experiment or theory for their strengths and positions. The vortex pair is then imaged inside the round body. Potential vortices have the whole vorticity concentrated at the vortex center and the flow is everywhere else irrotational. An indication of the accuracy of this model can be obtained from the experimental data by examining how the

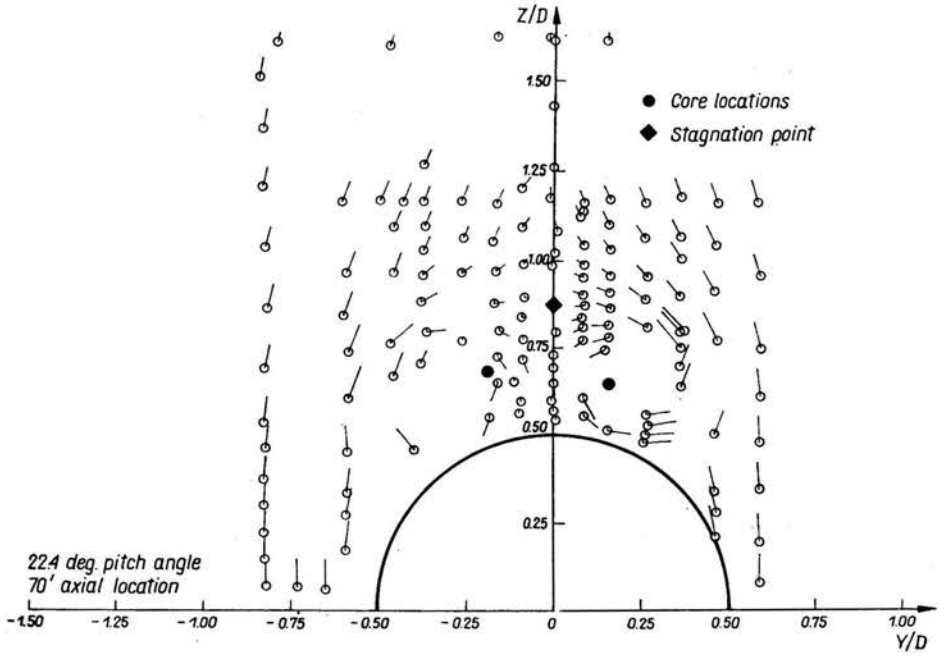

FIG. 3. Crossflow velocity field at $X/L = 0.70$.

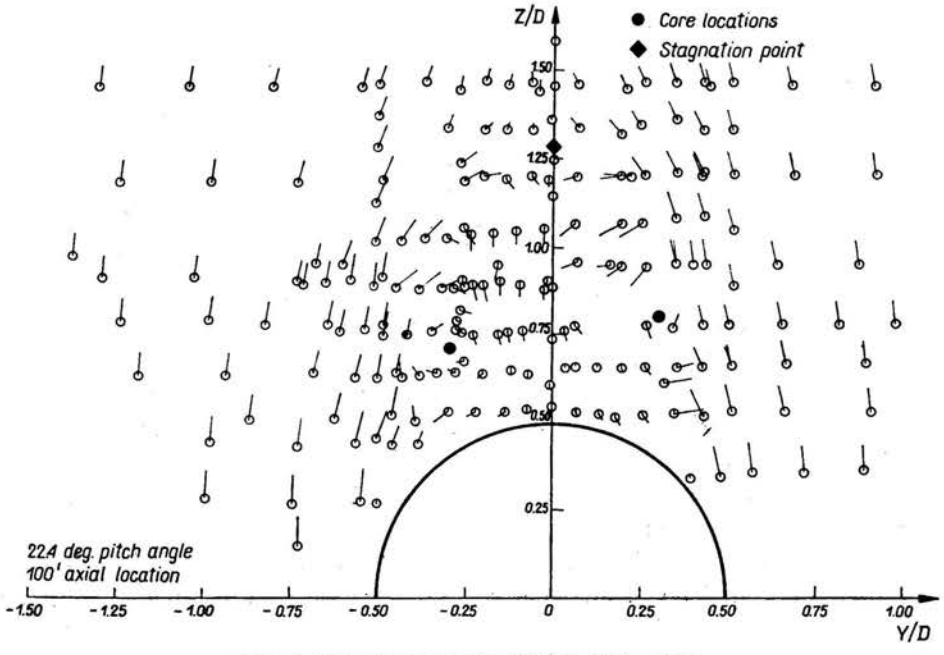

FIG. 4. Crossflow velocity field at $X/L = 1.00$.

vorticity is distributed in the crossflow planes. For this purpose, the plane at $X/L = 0.7$ was arbitrarily divided up into several domains as shown in Fig. 5. The circulation around the contours of the several domains was determined numerically. It is seen that out of the total vorticity on the left or right sides, about 92 percent is contained within the domain I or II which contain the vortex cores. The vorticity in the domains I and II is probably

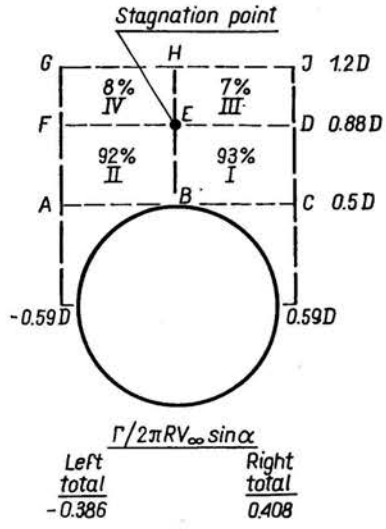

FIG. 5. Circulations from contour integrations (percentage of total in each contour), $X/L = 0.70$, $\alpha = 22.4°$.

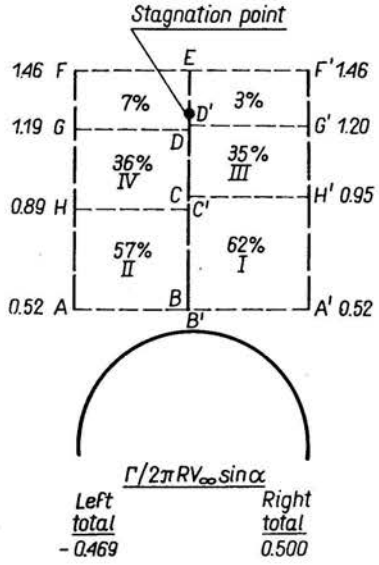

FIG. 6. Circulations from contour integrations (percentage of total in each contour), $X/L = 1.0$, $\alpha = 22.4°$.

dispersed but further breakdown of these domains was not made. A symmetric vortex pair can possibly model this flow fairly well.

In Fig. 6 results similar to those of Fig. 5 are presented for a plane normal to the body at its base. It is seen in this case that the domains I and II containing the vortex cores account for a smaller fraction of the total vorticity. A symmetrical vortex pair would thus not accurately model this flow. Whether the diffusion of vorticity in this case is increased by upstream influence of the base flow is not known. Repeating the measurements with a cylindrical extension to the body may give an answer to this question.

4. Comparison of symmetric vortex measurements with existing prediction methods

Let us now consider how existing prediction methods compare with the symmetric vortex measurements with regard to vortex strengths and positions. Figure 7 presents the comparisons for $X/L = 0.7$ and $\alpha = 22.4°$. With regard to the vortex position, the correlation curves of reference 14 were used for obtaining the vortex core coordinates. The figure shows also the FÖPPL line [15] giving vortex position if the vortex strength is known. Predicted vortex strengths from several methods are compared with experiment in Fig. 7. The methods considered are the Föppl theory based on potential flow [15], the correlation

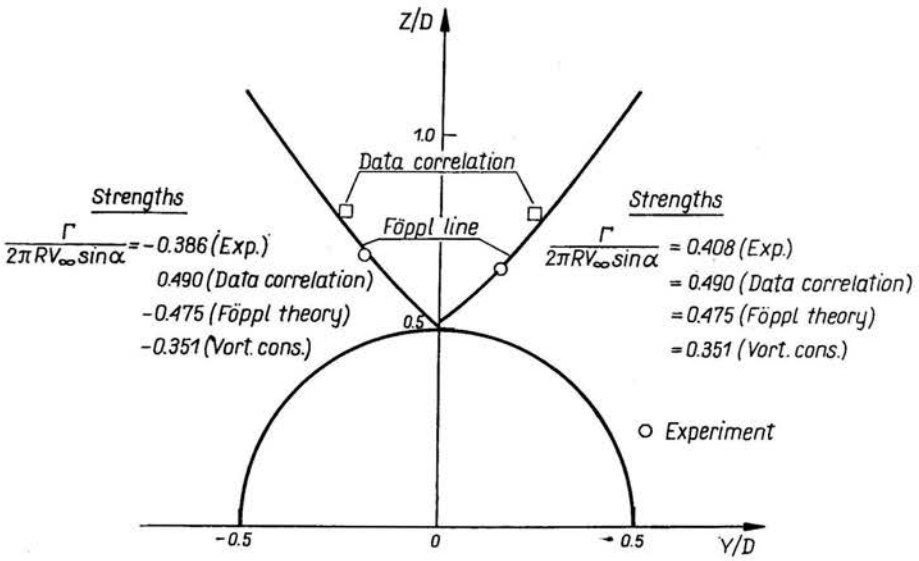

FIG. 7. Comparison of experimental and predicted vortex locations and strengths, $X/L = 0.7$, $\alpha = 22.4°$.

curve method [14], and the vorticity-conservation method of FIDLER [16]. Figure 7 shows that the vortices lie practically on the Föppl line, but this is thought to be coincidental. The positions predicted by Ref. [14] are not very accurate. With regard to vortex strength, the vorticity conservation method seems most accurate. The Föppl vortex strength was taken to be that corresponding to the point on the Föppl line nearest to the vortex core.

Figure 8 shows for $X/L = 1.0$ at $\alpha = 22.4°$, the same general results as the preceding figure. However, the vortices are now more asymmetric.

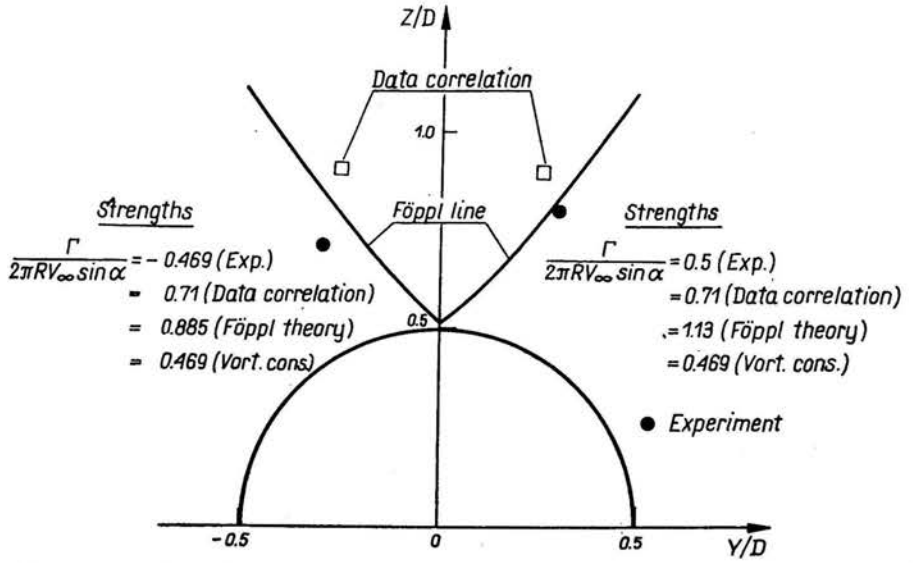

FIG. 8. Comparison of experimental and predicted vortex locations and strengths, $X/L = 1.0$, $\alpha = 22.4°$.

Comparison are presented in Ref. [11] between the potential theory and downwash measurements along certain lines in the flow field at $X/L = 0.7$ and 1.0. The theoretical results were obtained by using the experimental vortex strengths in the potential theory. It is shown that a symmetric vortex pair model predicts the flow fields fairly well at $X/L = 0.7$ but poorly at $X/L = 1.0$. The results indicate that more vortices must be used in the modeling to account for the fact that the vorticity is distributed rather than concentrated.

5. Vortex cloud theory

5.1. Crossflow analogy

The basic notion of the vortex cloud theory is to model the distributed vorticity fields exhibited by the circulation measurements of Figs. 5 and 6 by clouds of discrete potential vortices instead of just a symmetrical pair and to use boundary-layer methods to obtain separation positions and vortex strengths. This approach also leads to the possibility of handling asymmetric vortex fields. We now describe the theory.

Underlying the approach is the analogy between two-dimensional unsteady flow past a circular cylinder and the steady three-dimensional flow past an inclined body of revolution. This analogy was explained in connection with the von Kármán vortex street appearance of the flow in the crossflow of an inclined body of revolution shedding asymmetric vortices. The analogy assumes, in the case of a body of revolution, that there is no upstream influence of the body on the vortex formation in a given crossflow plane. This assumption can be overcome by modeling the body using three-dimensional sources and doublets when determining the body pressure distribution. Since the point vortices in the crossflow plane are equivalent to infinite rectilinear vortices, some upstream influence of the wake is also included.

5.2. Boundary-layer separation

The potential pressure distribution is computed on the body of revolution at the angle of attack using three-dimensional sources and doublets, and the full Bernoulli equation The boundary layer is now tested for separation by looking at its development in crossflow planes. At various values of axial distance starting from the nose, the boundary layer is tested for separation using modifications of the STRATFORD [8 and 9] criteria. The actual criteria used are:

$$\text{laminar:} \quad (C_p)^{1/2}\left(\xi \frac{dC_p}{d\xi}\right) = 0.087 \sin\alpha,$$

$$\text{turbulent:} \quad \frac{C_p\left(\xi \dfrac{dC_p}{d\xi}\right)^{1/2}}{(\mathrm{Re}_\xi/10^6)^{0.1}} = 0.35 \sin\alpha,$$

$C_p \dfrac{p - p_{\min}}{q_{\min}}$ local pressure coefficient,

$p_{\min}$ static pressure at minimum pressure point,

p local static pressure,
q_{min} dynamic pressure at minimum pressure point,
ξ distance from virtual origin of the boundary layer.

It is noted that the scale of ξ does not change the laminar separation criterion and has a 1/10 root effect on the turbulent separation criterion.

The Stratford criteria were originally developed assuming that a length of constant pressure flow on a flat plate suddenly encounters a length of rising pressure causing separation. Accordingly, the boundary-layer displacement thickness was calculated at the minimum pressure point on the side of the cylinder. This thickness was used to determine the equivalent length of the flat plate run up to the minimum pressure point and thereby to establish the virtual origin of ξ. The $\sin\alpha$ terms are not in the original Stratford criteria but have been arbitrarily added to bring predicted separation points for inclined bodies of revolution into agreement with the measured points [17]. This preliminary scheme may require further verification.

5.3. Starting vortex strengths and positions

The strengths of the vortices at the separation points are determined from boundary-layer considerations. The velocity profile approaching the separation point in the cross-flow plane is given by $v(r)$ from R to $R+\delta$. The vorticity transport per unit length of the body is given closely by

$$\frac{d\Gamma}{dt} = \int_R^{R+\delta} v \frac{\partial v}{\partial r}\, dr = \frac{V_\delta^2}{2}$$

or

$$\frac{d\Gamma}{dX} = \frac{1}{V_\infty \cos\alpha}\frac{d\Gamma}{dt} = \frac{1}{V_\infty}\frac{V_\delta^2}{2\cos\alpha}.$$

It has been found experimentally that this vorticity is not wholly captured in the recirculation region behind the cylinder [18]. Only a fraction, Λ, of some 50 to 60 percent is captured. What happens to the rest is not clear. It can, in part, be cancelled by vorticity annihilation between vorticity of different sign from either side of the cylinder, or it may just be convected past the recirculation zone on the outside. Finally, it may be offset by the rear shear layer vorticity of an opposite sign generated by the boundary layer approaching the stagnation point from the leeward side of the body. Accordingly, we now use

$$\frac{d\Gamma}{dX} = \frac{\Lambda}{\cos\alpha}\frac{1}{V_\infty}\left(\frac{V_\delta^2}{2}\right).$$

The quantity V_δ comes from the potential pressure distribution including the effects of any shed vorticity.

Knowing the shedding rate per unit length, $d\Gamma/dX$, we can eject small vortices into the flow for small increments in X, and calculate the paths of these vortices in a step-by-step marching procedure in X. The only remaining unknown quantity needed to carry out the procedure is the starting position of each incremental vortex. It is not possible to start the vortex too close to the body surface because the image vortex would give it too large an

initial tangential velocity. Basing on trial calculations, it has been found that the vortex should be put out along a radial line through the stagnation point by a distance ΔR determined in the following manner: Choose $\frac{\Delta R}{R} = 0.05$ or such that the separation point is a stagnation point of the flow, whichever gives the larger value. For the least value of X at which separation occurs, it does so near the top of the body. Thereafter the separation point moves down the side of the body as X increases. As vortices are started at the separation point, their paths are calculated step-by-step downstream and their influence on the pressure distribution is taken into account in subsequent vortex shedding since it changes the separation point and its associated quantities.

5.4. Computational problems

One problem frequently occurring in calculating the rolling up of a vortex sheet or the formation of vortex clouds as in the present case is that two potential vortices may approach each other too closely and induce unrealistically large velocities on each other. Two schemes have been used to avoid this problem. Rather than purely potential vortices, diffusive vortices of the same strength have been used. Such a vortex, described by MILNE-THOMSON [19], avoids singularity in velocity at the center of a potential vortex. The vortex then has an age, and the ageing is controlled by choice of viscosity. If, in spite of the use of diffusive vortices, the mutual interaction between closely spaced vortices becomes too great, they are combined at their centroid. The use of these two devices permits smooth calculation of the vortex cloud with fairly large $\Delta X/D$ increments; for example, $\Delta X/D = 0.165$ is used herein.

5.5. Asymmetric vortex clouds

The computational program has the property that if the initial vortices are not started symmetrically, the left- and right-hand clouds will develop asymmetrically at a rate depending on the original asymmetry. Eventually, one cloud will tear away from the cylinder, and another cloud will start to form under it just as is found experimentally. The solution for the asymmetric vortices is thus not unique in an a priori sense, but depends on the magnitude of the original displacement of the separation points. Figure 9 exhibits the behaviour of the vertical position of the centroid of the vortex clouds resulting from several initial displacements. The displacements were imparted to the vortices by displacing the right separation point upward by an amount $\Delta\theta_S$ from its symmetrical position and displacing the left separation point downward by $-\Delta\theta_S$. The length over which this asymmetry was introduced on the nose of the body is shown in the figure. The paths are shown of the vertical position of the vortex cloud centroid for three different initial displacements. They start at the point where the cloud breaks away from the body. It is noted that the larger the initial displacement, the higher the vortices are at the body base. Shown on the figure are the vortex core positions at $X/L = 0.7$. The displacement corresponding to $\Delta\theta_S = 2.5°$ yields vortex paths in fair agreement with the data points. Accordingly, this calculative case was used for comparison with the flow field data. In the present work, the

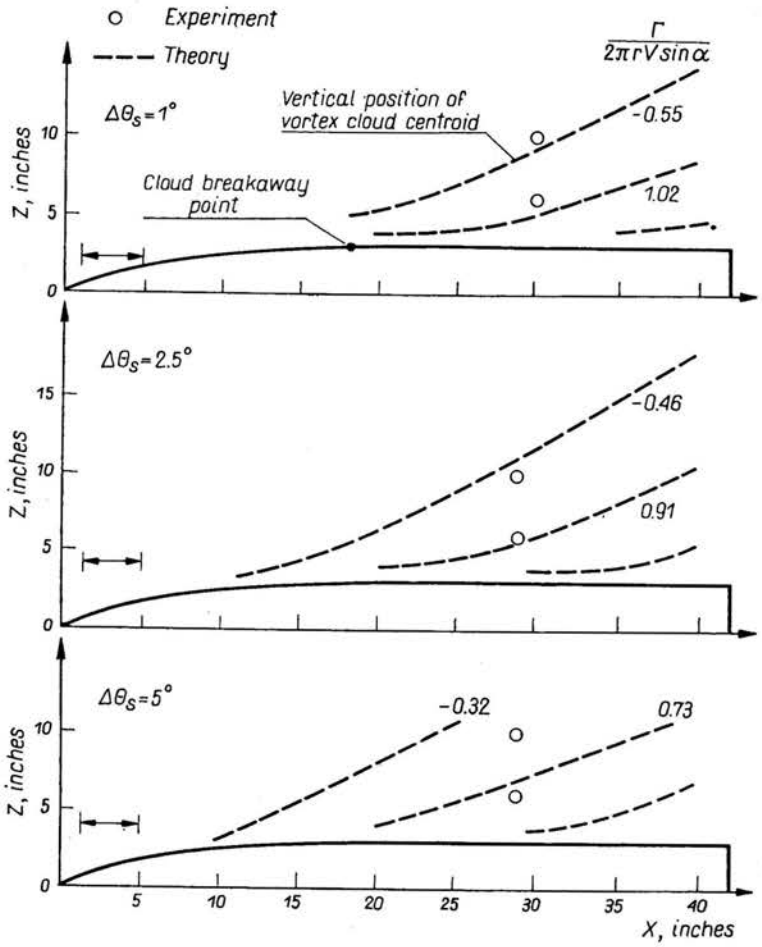

FIG. 9. Measured and predicted asymmetric vortex positions on $L/D = 7$, ogive-cylinder at $\alpha = 37.5°$.

experimental rate of onset of asymmetry may have depended on the degree of asymmetry introduced on the body by the use of a small piece of tape to make the asymmetric pattern steady. The fact that the degree of asymmetry depends on the magnitude of the initial asymmetry is not compatible with the notion that such asymmetry occurs due to the hydrodynamic instability of a symmetric vortex pair. This point needs further clarification.

6. Comparison between experiment and predictions of vortex cloud theory

6.1. Symmetric vortex case

Figure 10 shows the calculated vortex clouds for the case of $X/L = 0.7$ at $\alpha = 22.4°$. About a dozen vortices are shown in each cloud. In Fig. 11 it appears that separation starts at the top of the body and moves smoothly down the sides to asymptotic positions corre-

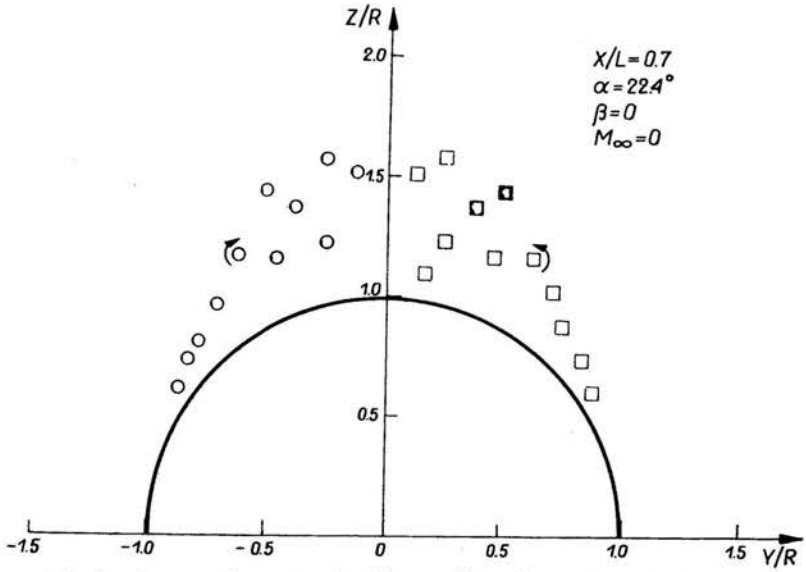

FIG. 10. Calculated symmetric vortex cloud in crossflow plane $L/D = 7$ ogive-cylinder.

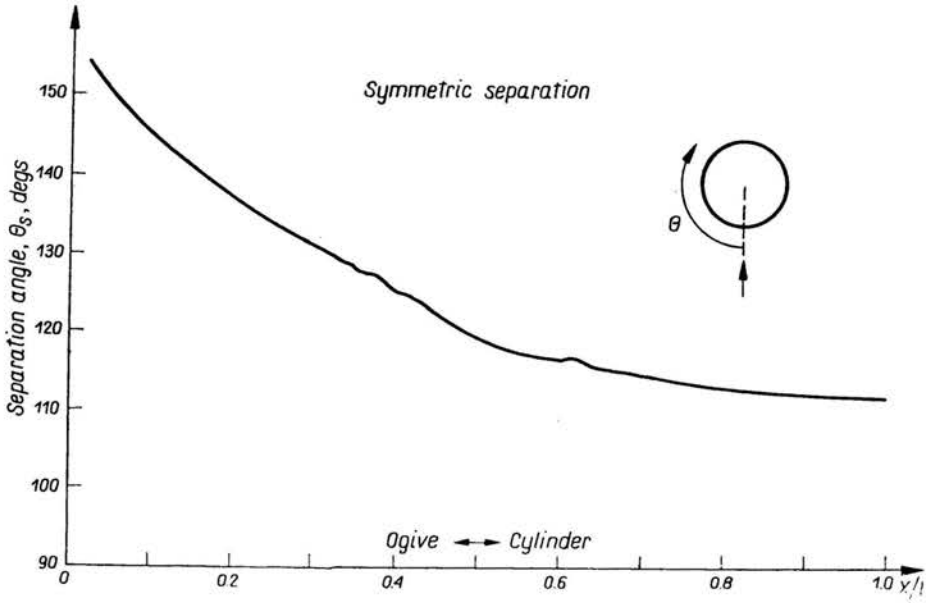

FIG. 11. Theoretical separation line location for ogive-cylinder at $\alpha = 22.4°$.

sponding to θ_S of about 113°. Figures 12, 13 and 14 show the agreement between measured and predicted downwash fields for the symmetric case. The degree of agreement in this and similar cases is generally good.

The calculated values of $\Gamma/2\pi RV_\infty \sin\alpha$ at $X/L = 0.7$ and 1.0 were ± 0.364 and ± 0.556, respectively, as compared with the mean experimental values of 0.397 and 0.485. Turbulent separation was assumed in the calculation.

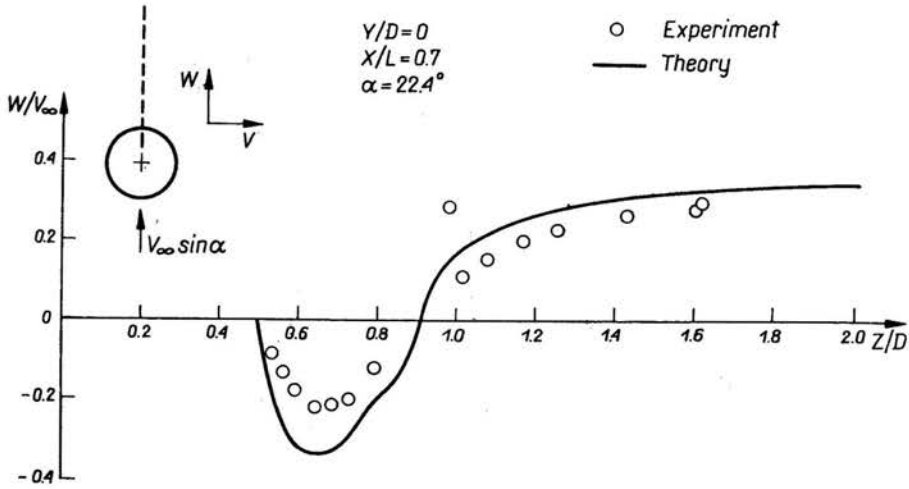

FIG. 12. Symmetric vortex flow field, vertical centerline.

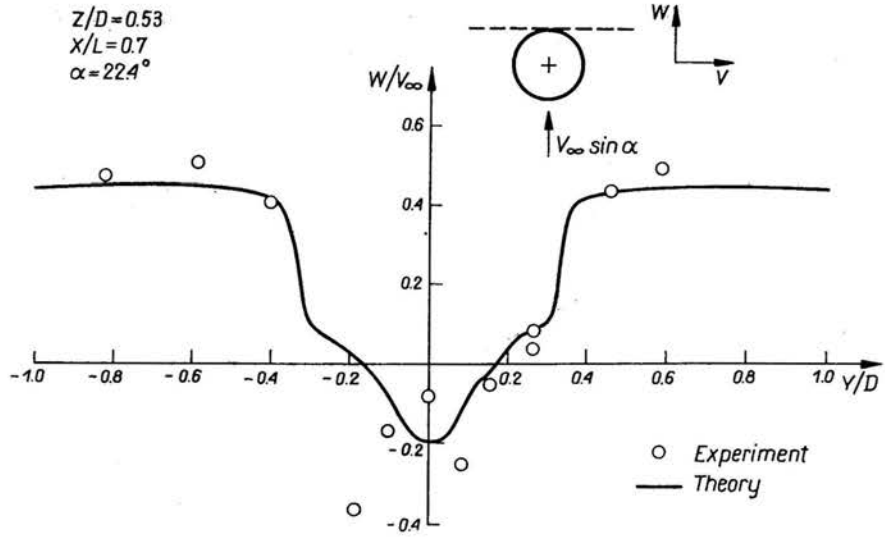

FIG. 13. Symmetric vortex flow field, $Z/D = 0.53$ traverse.

6.2. Asymmetric vortex case

Figure 15 shows the calculated vortex clouds for the case $X/L = 0.7$ and $\alpha_c = 37.5°$. The upper left-hand cloud has torn away from the body and is now free. The total number of vortices on the left and right are not precisely the same because some vortices in close proximity have been combined.

Figure 16 shows the interesting behavior of the separation lines accompanying asymmetric vortex separation. Between $X/L = 0.48$ and 0.67, the left-hand vortex cloud separates from the body and a new vortex cloud starts forming. The new left-hand vortex

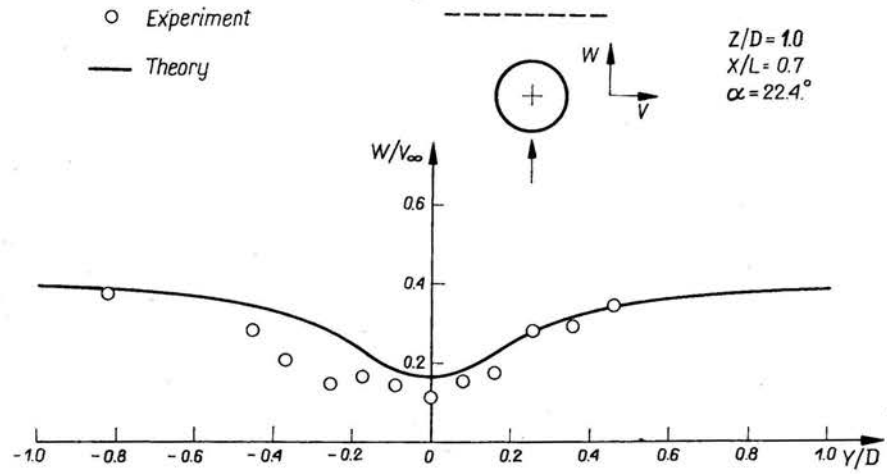

FIG. 14. Symmetric vortex flow field, $Z/D = 1.0$ traverse.

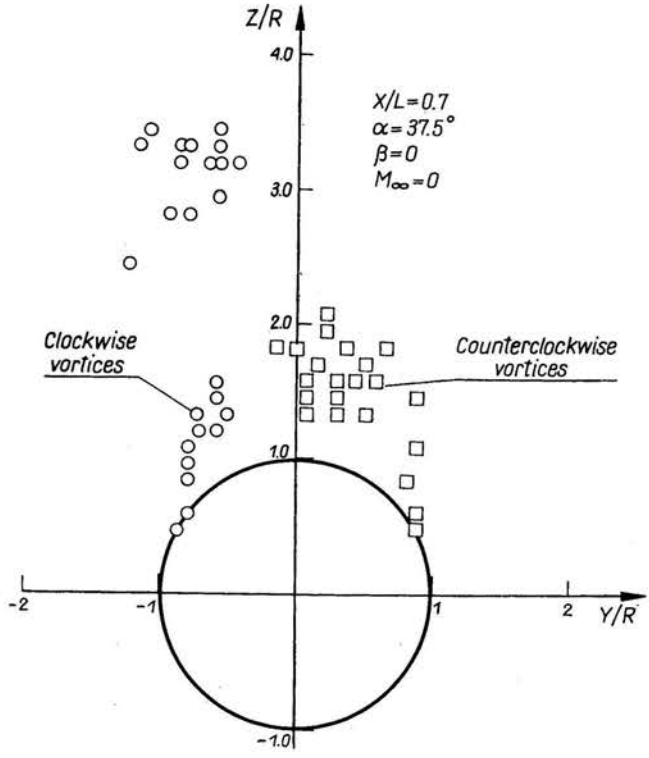

FIG. 15. Calculated asymmetric vortex cloud in crossflow plane $L/D = 7$ ogive-cylinder.

cloud is then very weak and cannot push the left-hand separation point very far down the side of the body. Accordingly, the left-hand vortex separation point now moves upward toward the top of the body. Between $X/L = 0.67$ and $X/L = 0.86$, a right-hand vortex

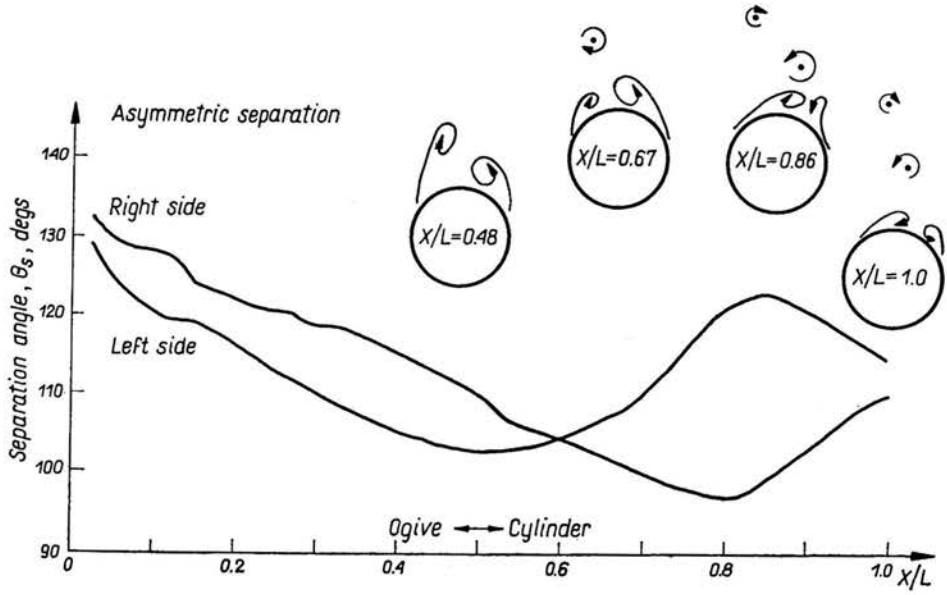

FIG. 16. Calculated separation line locations for ogive-cylinder at $\alpha = 37.50°$.

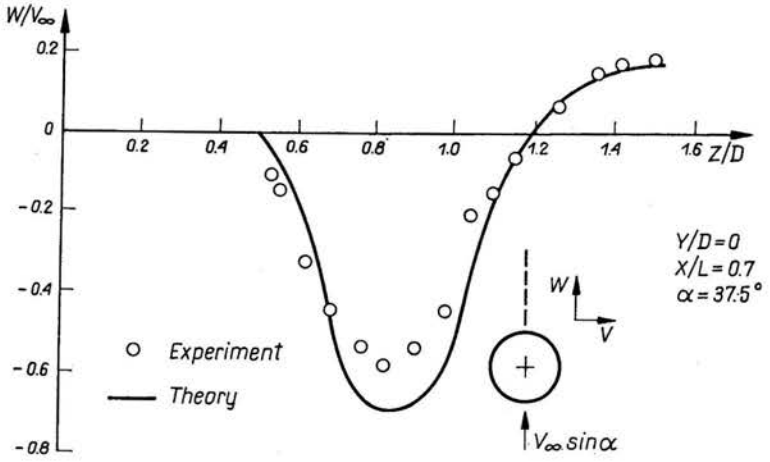

FIG. 17. Asymmetric vortex flow field. Vertical centerline.

cloud separates from the body and a new vortex cloud forms under it. The separation point will now move upward on the right side of the body while it is moving downward on the left side. A periodic solution has emerged. In Figs. 17-20 comparisons between experiment and theory for the asymmetric vortex flow field are shown. Generally the agreement is as good as for the symmetric case. The asymmetric vortex model thus not only contains the basic quantitative features of the measurements but is also in good quantitative agreement with them.

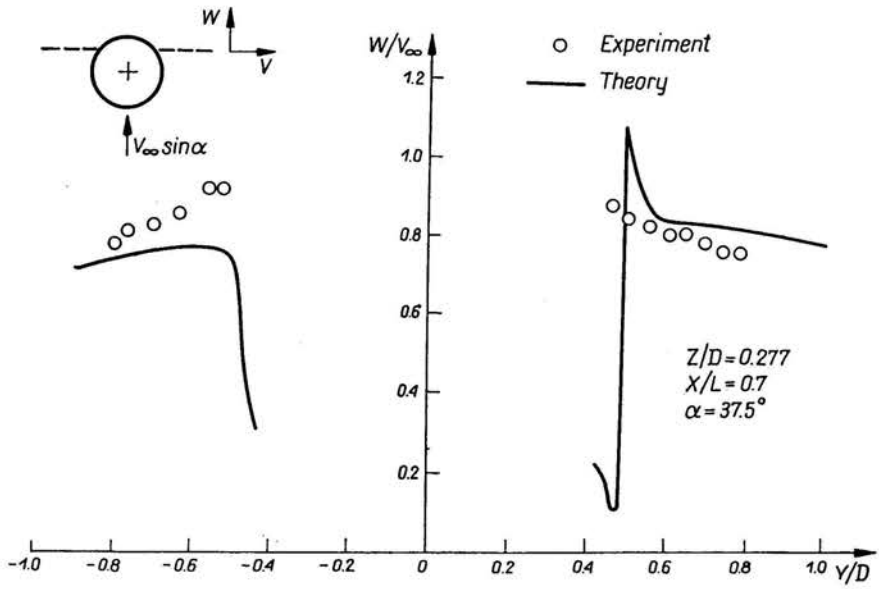

FIG. 18. Asymmetric vortex flow, $Z/D = 2.77$ traverse.

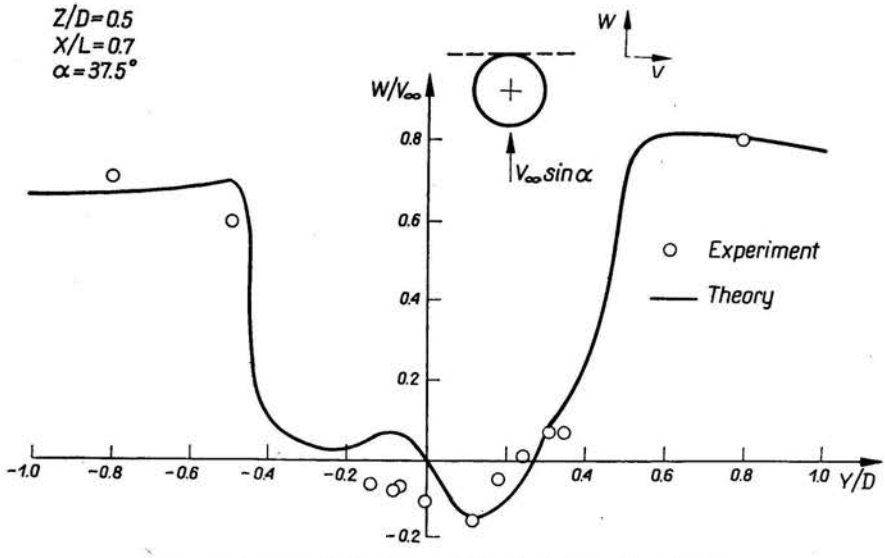

FIG. 19. Asymmetric vortex flow field, $Z/D = 0.5$ traverse.

7. Concluding remarks

An experimental and analytical study has been made of the velocity field associated with symmetric and asymmetric vortex shedding from an inclined body of revolution at incompressible speed. With the use of a laser Doppler velocimeter, detailed flow measure-

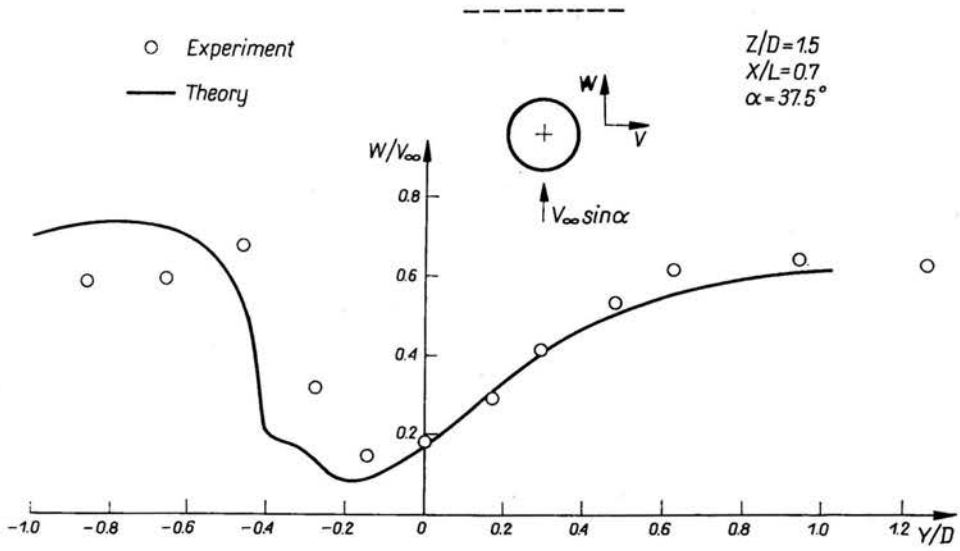

FIG. 20. Asymmetric vortex flow field, $Z/D = 1.5$ traverse.

ments were made of the downwash and sidewash velocities in two planes normal to the body axis, including the plane of the base. At an angle of attack of 22.4° the vortices were closely mmetric. At an angle of attack of 37.5°, the vortices were asymmetric; however, it was necessary to place a strip of tape on the side of the body nose to stabilize the flow and obtain detailed measurements.

The velocity field data were used to determine the circulation associated with certain arbitrary contours on the leeward side of the body. It was found that contours not containing vortex centers did not have zero circulation indicating that the vorticity was not concentrated. In the plane at the base of the body, the vorticity was more diffuse than at the 70 percent body-length position.

Several different existing methods were used to predict total measured vorticity including the Föppl solution, data correlation curves, and the vorticity conservation method. The vorticity conservation method gave the best predictions. The vortex positions were predicted only fairly well. Experimental vortex center positions and measured vortex strengths were used in a potential symmetrical vortex pair model of the flow for predicting flow field components. For $\alpha = 22.4°$ at the 70 percent body station, the predictions were in good agreement with experiment. The predictions in the plane of the base are generally not good, indicating that a multivortex model is required.

A predictive computer method based on a multivortex approach is described for both symmetric and asymmetric vortex separation. This approach yields a priori predictions for symmetric vortices. For asymmetric vortices, an initial disturbance must be given to the vortices. The amount of disturbance depends on the magnitude of the actual asymmetry producing the asymmetric vortices. Comparison between predicted and measured flow fields are made for both cases. It is found that both the asymmetric and symmetric flow fields are well predicted by the multivortex method.

References

1. K. D. THOMSON and D. F. MORRISON, *The spacing, position and strength of vortices in the wake of slender, cylindrical bodies at large incidence*, J. Fluid Mech., **50**, 4, 751–783, 1971.
2. L. FÖPPL, *Wirbelbewegung Hinter einen Kreiszylinder*, Sitzbericht der Bayerischen Akademie der Wissenschaft, 1913.
3. E. BRYSON jr., *Symmetric vortex separation on circular cylinders and cones*, J. Appl. Mech., 643–648, 1959.
4. S. B. ANGELUCCI, *A multivortex method for axisymmetric bodies at angle of attack*, J. Aircraft, **8**, 12, 959–966, 1971.
5. A. B. WARDLAW jr., *Prediction of normal force, pitching moment, and yaw forces on bodies of revolution up to 50 degree using a concentrated vortex flow-field model*, NOL TR 73–209, Oct. 1973.
6. D. KUHN, *Evaluation of a theoretical method for calculating side-force onset on bodies of revolution*, Nielsen Engineering and Research, Inc., TR 96, 1975.
7. F. J. MARSHALL and F. D. DEFFENBAUGH, *Separated flow over bodies of revolution using an unsteady discrete-vorticity cross wake, Part 1. Theory and application*, NASA CR-2415, June 1974.
8. L. ROSENHEAD, *Laminar boundary layer*, Oxford Univ. Press, 324–331, 1963.
9. B. S. STRATFORD, *The prediction of separation of the turbulent boundary layer*, J. Fluid Mech., **5**, 1–16, 1956.
10. J. E. FIDLER, R. G. SCHWIND and J. N. NIELSEN, *An investigation of slender-body wake vortices*, NEAR TR 108, 1976.
11. J. E. FIDLER, R. G. SCHWIND and J. N. NIELSEN, *An investigation of slender-body wake vortices*, AIAA Paper 77-7, presented at the AIAA 15th Aerospace Sciences Meeting, Jan. 24–27, 1977.
12. W. J. YANTA and A. B. WARDLAW, *Laser Doppler velocimeter measurements of leeward flow fields on slender bodies at large angles of attack*, AIAA Paper 77–660, presented at AIAA 10th Fluid and Plasmadynamics Conference, Albuquerque, June 27–28, New Mexico 1977.
13. R. G. SCHWIND and D. M. KLINE, *Data report on laser anemometer measurements of missile body-separation vortices*, NEAR TR 91, June 1975.
14. M. R. MENDENHALL and J. N. NIELSEN, *Effect of vortex shedding on the longitudinal aerodynamic characteristics of wing-body-tail combinations*, NASA CR-2473, Jan. 1975.
15. J. N. NIELSEN, *Missile aerodynamics*, McGraw-Hill, 91–94, 1960.
16. J. E. FIDLER, *Approximate method for estimating wake vortex strength*, AIAA, **12**, 5, 633–635, 1974.
17. B. E. TINLING and C. Q. ALLEN, *An investigation of the normal-force and vortex-wake characteristics of an ogive-cylinder body at subsonic speeds*, NASA TN D-1297, April 1962.
18. A. FAGE and F. C. JOHANSEN, *The structure of vortex sheets*, Phil. Mag. S.7, **5**, 28, 417–441, 1928.
19. L. M. MILNE-THOMSON, *Theoretical hydrodynamics*, 5th Edition, The McMillan Company, 666, New York 1968.

NIELSEN ENGINEERING AND RESEARCH, INC.,
MOUNTAIN VIEW, CA USA.

Received September 27, 1977.